Available online at www.sciencedirect.com
SCIENCE DIRECT®
International Journal of Heat and Fluid Flow 25 (2004) 364–372
International Journal of HEAT AND FLUID FLOW
www.elsevier.com/locate/ijhff

Vortex shedding from two surface-mounted cubes in tandem

Robert J. Martinuzzi *, Brian Havel

Advanced Fluid Mechanics Research Group, Department of Mechanical and Materials Engineering, Faculty of Engineering, University of Western Ontario, London, ON, Canada N6A 5B9

Abstract

Periodic vortex shedding from two surface-mounted cubes, of height H, in tandem arrangement placed in a thin boundary layer is investigated for a spacing 2H using phase-averaged Laser Doppler Velocimetry. Tests were conducted for a Reynolds number of 22,000, based on H and the freestream velocity, and an approximately $0.07H$ thick laminar boundary layer. For obstacle separations between $1.5H$ and $2.5H$, the shedding frequency scales inversely with the obstacle spacing, S, such that the Strouhal number based on S is constant or geometrically locked. In this locked regime, periodic shedding is triggered by the interference between a vertical flow stream along the front face of the downstream obstacle and the vortex in the inter-obstacle cavity. This three-dimensional mechanism is not observed for two-dimensional geometries and helps explain why a locked regime cannot be observed for square cylinders in tandem arrangement. Furthermore, it is shown that the structure of the turbulent field in the cavity region differs significantly from that in the base region of a two-dimensional obstacle.

Keywords: Vortex shedding; Tandem surface-mounted cubes; Phase-averaging; Turbulence; Experimental; Bluff-body interference

1. Introduction

The flow around multiple bluff bodies has been extensively studied due to its practical significance in many engineering applications, for example, in determining dynamic loading on neighboring structures or the influence on heat transfer and dispersion. An important mechanism for flow-structure interaction is the coupled interference between the obstacles on the vortex formation and shedding process.

Rockwell (1998) provides an encompassing review of the studies conducted for two-dimensional bluff bodies. When an obstacle undergoes forced periodic oscillations, the shedding frequency can lock on to the obstacle oscillation frequency, if the two are not too different. Gaydon and Rockwell (1999) have shown that, for a fixed obstacle, incident vortices can dramatically shorten the formation length in the cylinder wake and thus modify the vortex shedding frequency, which can also result in lock-on. Similarly, when two cylinders are placed in tandem in a uniform stream, the shedding frequency from the second obstacle can lock on to that of the first obstacle over a critical obstacle spacing range (cf. Zdravkovich, 1977; Albrecht et al., 1988). As the spacing between the obstacles is changed, up to four regimes have been identified for both circular (Zdravkovich, 1977) and square cylinders (Hangan and Vickery, 1999) in tandem arrangement. For very small obstacle separation, the flow is similar to that for a single bluff body. For intermediate separations, there is a region of bistable flow, for which two non-harmonic frequencies are reported. Each frequency is associated with a different mode of motion and occurs intermittently. Okajima (1982) reported a similar behavior for two-dimensional, rectangular bluff bodies of sufficiently large streamwise-to-cross-sectional length aspect ratios. For larger separations, the shedding frequency from the second obstacle locks on to that of the first. For very large separations, the obstacles shed independently.

Three-dimensional geometries have received much less attention, possibly because these often occur deep in boundary layers and periodic vortex shedding is suppressed. However, if the boundary layer thickness is less than approximately 70% of the body height, vortex shedding is observed (cf. Castro and Robins, 1977; Sakamoto and Haniu, 1988). For surface-mounted rectangular bluff bodies in tandem arrangement, small separation (intermittent), lock-on and large separation

* Corresponding author. Tel.: +1-519-661-2111; fax: +1-519-661-3020.
E-mail address: rmartinuzzi@eng.uwo.ca (R.J. Martinuzzi).

0142-727X/$ - see front matter © 2004 Elsevier Inc. All rights reserved.
doi:10.1016/j.ijheatfluidflow.2004.02.003

regimes similar to those for the two-dimensional geometries have been reported by Sakamoto and Haniu (1988) and Havel et al. (2001). However, Martinuzzi and Havel (2000) have shown that the three-dimensional geometry shows a critical range, between the intermittent and the lock-on regimes, where the shedding frequency scales inversely with the obstacle spacing. Effectively, the shedding frequency is locked to the inter-obstacle cavity geometry.

In this work, the flow in the cavity between two surface-mounted cubes in the locked regime is investigated for the purpose of understanding why the shedding frequency scales with the obstacle gap and why a similar regime is not observed for two-dimensional obstacles in tandem arrangement. The cubes are mounted two obstacle heights apart and placed in a thin boundary layer. Based on surface pressure and laser Doppler velocimetry measurements, mean and phase-averaged representations of the flow field are used to investigate the shedding process in greater detail and to discuss some aspects of the turbulence field.

2. Experimental details

The flow was produced in an open, suction-type wind tunnel with a honeycomb and several fine grids at the inlet. Air flowed through a 4:1 contraction into a 0.46×0.46 m^2 test section. The inlet profile was uniform within 1% of the free stream velocity, U = 8.8 m/s, and the free stream turbulence intensity was less than 1.5% as measured with a hot-wire anemometer. The experimental set-up and nomenclature are shown schematically in Fig. 1. Two cubes of dimension $H = 0.04$ m were mounted on a thin (3 mm) flat plate along the streamwise line of symmetry of the test-section at a distance of $2H$ from the leading edge. A plate end-flap was adjusted to control separation at the plate leading edge and maintain a thin boundary layer. The Reynolds number based on cube height, H, and free-stream velocity, U, was 22,000. The on-coming boundary layer was laminar and matched the Blasius profile. At the mounting point of the first cube, $x = 2.5H$, the boundary layer thickness was $\delta/H \approx 0.07$.

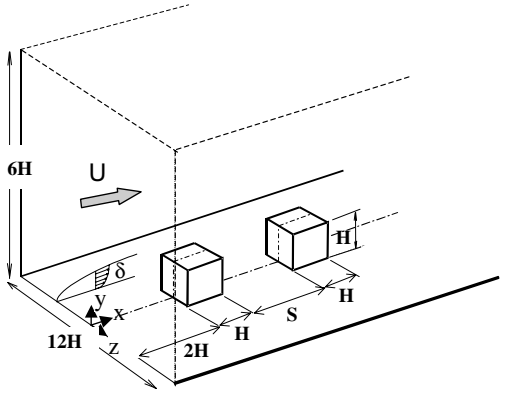

Fig. 1. Schematic representation of the set-up and nomenclature.

Surface pressure measurements were made at several locations on the plate and cube surfaces. The pressure taps were 0.7 mm in diameter. The reference was taken as the free-stream static pressure from the pitot static tube. The frequency response of the system (pressure tap, tubing, and sensor) was flat to 200 Hz. The transducer resolution was ±0.5 Pa and data was sampled at 2 kHz.

Velocity data were acquired with a two-component, TSI series 9000, fiber optic Laser Doppler Velocimetry (LDV) system. The optical setup consisted of a 0.453 m focal length lens with a $2.6\times$ beam expander resulting in an effective measurement volume of diameter 46 μm and length 340 μm. The LDV processor was a two channel TSI IFA 655 correlator operated in single-measurement-per-burst (SMB) mode. The coincidence window between the two velocity channels was set to 200 μs, based on preliminary measurements at several locations showing the shear stress coefficient was insensitive to the coincidence window setting in the range 50–500 μs. A frequency shift of 5 MHz was applied to both measurement channels to eliminate directional ambiguity.

The flow was seeded upstream of the honeycomb with an atomized 10:1 water–glycerol mixture. The particle number mean diameter was 4 μm with 90% of the particles being less than 8 μm. Following Rudoff and Bachalo (1991), these particles are expected to follow the flow.

The phase-averaged velocity field was analyzed subject to the triple decomposition:

$$U_i^* = u_i + u_{ci} + u_i'$$

where: U_i^* is the instantaneous velocity, u_i is the local long-time mean, u_{ci} is the fluctuating coherent (phase-average) and u_i' is the turbulent (incoherent) contribution. The subscript i indicates the physical velocity component: u (streamwise), v (vertical), and w (spanwise). The common reference event for all data points was taken as the peak pressure during each shedding period measured on the side face of the upstream cube. Individual cycle periods were determined from the peak-to-peak time differences. The velocity data were then redistributed over 20 equally spaced bins to reconstruct a phase-averaged cycle. The phase-averaged operation is denoted by $\langle\cdots\rangle$ and represents the transit-time weighted average within each bin for the first and second moments:

$$\langle u_i\rangle = \langle U_i^*\rangle = u_i + u_{ci} \quad \text{and} \quad \langle u_i' u_j'\rangle,$$

where the subscripts i and j indicate the component, as well as turbulence kinetic energy written explicitly as

$$\langle k\rangle = \frac{1}{2}\lfloor\langle u'^2\rangle + \langle v'^2\rangle + < w'^2 >\rfloor.$$

Mean and phase-averaged measurements of the three velocity components were made in ten normal and horizontal planes, each containing between 300 and 1100 measurement points. Typical data rates, N, ranged from 200 Hz, in the base regions, to 5 kHz in the shear layers. The average shedding frequency was approximately 23 Hz. At each point, data was collected for at least 50,000 LDV-events or 1000 shedding cycles. Only two perpendicular velocity components could be recorded simultaneously. It was thus necessary to measure each plane twice to obtain the three velocity component pairs u, v and u, w. The redundant data, usually the streamwise component, u, were used to verify repeatability and uncertainty estimates.

The Taylor micro time scale, T_λ, was estimated at several stations in the flow field from the autocorrelation function of the streamwise velocity. The effective data density, NT_λ, was greater than 5 everywhere, which according to Edwards (1987) ensures very low velocity bias when using transit-time weighting. The velocity uncertainty was estimated to be 1% in the mean and 5% for phase-averaged statistics in a 95% confidence interval (cf. Benedict and Gould, 1996). These estimates were verified using the redundant u-velocity measurements. Further verification was obtained by re-processing selected velocity data using the pressure reference signal on the side face of the downstream cube. Again, these results agree within the estimated uncertainty bounds. The measurement volume was positioned using a three-axis traversing platform accurate to 10 μm/m.

3. Results

For low aspect ratio, square cross-section, surface mounted obstacles arranged in tandem, Sakamoto and Haniu (1988), for obstacles $3H$ high, and Martinuzzi and Havel (2000), for cubes, identified four distinct shedding regimes on the obstacle spacing, S. The average vortex shedding frequency, f, measured downstream of two cubes is shown in Fig. 2 as a function of S/H and is expressed in terms of the non-dimensional Strouhal number based H, $St_H = fH/U$, and the spacing, $St_S = fS/U$. For the intermittent regime, $S/H < 1.5$, vortex shedding is interrupted by periods of random fluctuations. For the cavity locked regime, $1.5 < S/H < 2.5$, vortex shedding is continuous and the frequency scales inversely with S. For $4 < S/H < 6$, shedding from the downstream cube locks on to those vortices shed from the upstream cube, giving rise to a strong harmonic signal. For larger obstacle separations, the cubes shed independently and the shedding frequency asymptotically approaches the value for isolated cubes.

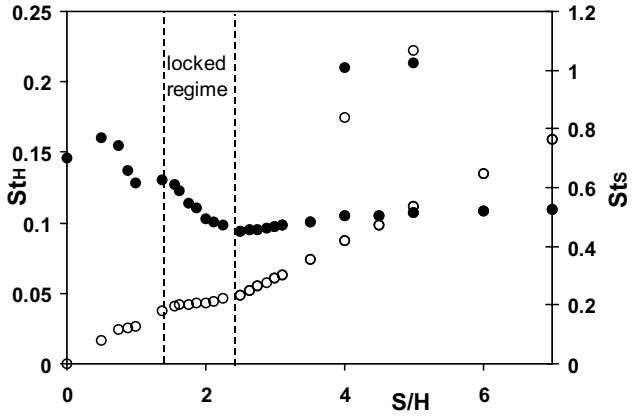

Fig. 2. Shedding frequency measured downstream of the second cube in terms of the non-dimensional Strouhal numbers based on H, St_H (closed symbols), and on S, St_S (open symbols), as functions of the gap size, S.

For the analogous, two-dimensional geometry, i.e. square cross-section cylinders in tandem in a uniform stream, a cavity locked regime is not observed and there is an abrupt transition from intermittent to continuous vortex shedding regimes occurring at $S/H \approx 2$ (cf. Havel et al., 2001).

The differences in flow behavior can be conveniently summarized from the changes in the drag coefficient, C_D based on the frontal area and free-stream velocity, measured for the two obstacles as a function of spacing as shown in Fig. 3. For the two-dimensional geometry, C_D for both obstacles shows an abrupt drop at $S/H \approx 2$. This spacing coincides with the sudden transition from intermittent to continuous periodic shedding. For larger spacing, C_D for the first obstacle is approximately that for the single body in a uniform stream ($C_D \approx 2.1$). The lower C_D-value for the second body for $S/H > 2$ results from the reduced flow speed in the wake of the upstream obstacle.

In contrast, for the three-dimensional geometries, the drag coefficient varies smoothly from the intermittent to the continuous shedding regimes. For the upstream obstacle, C_D initially decreases as S/H increases, reaching a minimum approximately at the end of the cavity locked regime. For the downstream obstacle, the end of this regime is marked by an inflection in the C_D vs. S/H curve.

To elucidate why a cavity locked regime is observed for three-, but not two-dimensional, tandem geometries requires a detailed investigation of the velocity field. First, the mean velocity field will be described to highlight some of the marking features in the locked regime. Subsequently, the shedding mechanism will be discussed in light of the velocity fields at different phases of the shedding cycle.

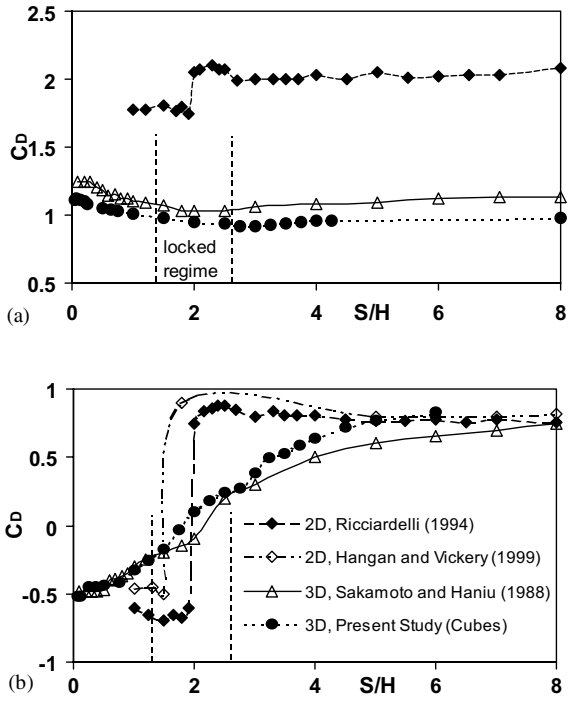

Fig. 3. Drag coefficient, C_D, vs. S/H for (a) upstream and (b) downstream obstacles in tandem arrangements of square cross-section obstacles. Data shown are those of: Ricciardelli (1994) and Hangan and Vickery (1999) for tandem square cylinders; Sakamoto and Haniu (1988) for surface-mounted prisms of height $3H$; and of the present study for surface-mounted cubes.

The flow field for two cubes in tandem at a spacing of $S/H = 2$ is representative for the cavity locked regime ($1.5 < S/H < 2.5$). The mean velocity components in the plane of symmetry, $z/H = 0$, and in the horizontal plane, $y/H = 0.375$, are shown as vectors in Fig. 4. A similar mean flow topology is observed in the horizontal planes $0.05 < y/H < 0.75$. For clarity, the wall refers to the solid boundary along $y/H = 0$, the roof is the cube face along $y/H = 1$, the upper and lower sides refer to the cube faces along $z/H = -0.5$ and 0.5, respectively.

From Fig. 4(a), the dividing streamline in the separated shear layer, originating at the upstream cube leading edge, impinges at the leading edge of the downstream cube roof. The dividing streamline attaches to the leading edge of the roof. There is a strong vertical flow directed towards the wall along the front face, while the flow over the roof is attached in the mean as well through the shedding cycle. This flow pattern is similar through the locked regime.

In the horizontal plane, Fig. 4(b), the large, counter-rotating recirculation vortices between the obstacles, with foci labelled $V1$ and $V2$, and the two saddle points, $S1$ and $S2$, are the principal topological features of interest. As is discussed below, circulation is periodically advected downstream from these vortices, in alternating fashion, to form a vortex street in the wake. The two saddle points mark the maximum mean downstream extent of these vortices. These form due to the interference between the recirculation vortices and the

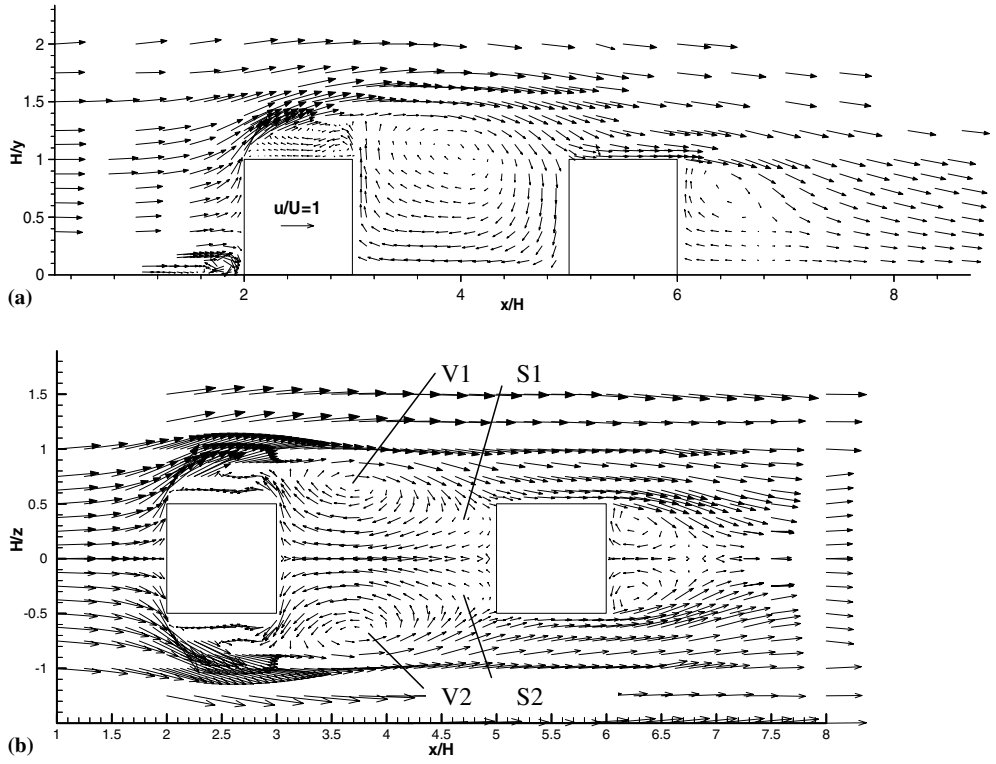

Fig. 4. Mean flow representation in vector form for tandem cubes of spacing $S/H = 2$: (a) plane $z/H = 0$; (b) plane $y/H = 0.375$.

vertical flow along the windward face of the downstream obstacle. This three-dimensional effect cannot exist in the case of the tandem square cylinder geometry. Also note that the flow along the side faces of the downstream obstacle is attached.

The flow patterns for other S/H was investigated by Martinuzzi and Havel (2000). For $S/H < 1.5$, the dividing streamline of the shear layers generated at the upstream cube leading edges attach on the roof and side faces (downstream of the leading edges) of the downstream cube. Thus the downstream cube interferes with the flow of circulation (from the upstream cube) into the forming vortices in the cavity and disrupts the formation process, resulting in irregularly shed vortices. For $S/H > 3$, the separated shear layer attaches upstream of the second cube, forming a new horseshoe vortex at its base. A stagnation point appears on the front face of this cube and the strong downward vertical stream is no longer observed. This change results in higher pressures on the front face of the cube, which are observed as an increase in the drag coefficient, as shown in Fig. 3. The flow patterns around the upstream cube, however, change little and it is thus not surprising that the drag coefficient is insensitive to S/H (see Fig. 3). The saddle points $S1$ and $S2$ merge to form a single saddle point along the plane of symmetry, which marks the end of the formation region. The flow separates on the side faces of the downstream obstacle. For $3 < S/H < 6$, the shedding of vortices from the base of the downstream obstacle are synchronized with those shed from the first cube, resulting in a strong harmonic peak (see Fig. 2). For larger S/H, shedding from the two obstacles is no longer synchronized. In the following section, it is proposed that the triggering mechanism for vortex shedding in the locked regime is three-dimensional in nature and thus fundamentally different from the classical, two-dimensional model. The latter is comprehensively discussed by Williamson (1996) and is here only briefly summarized.

Consider the vortex formation process on a cylinder placed in a uniform flow from left to right. The shedding cycle, arbitrarily chosen to start with the formation of a vortex on the upper face, can be described as follows. The flow separates at the leading edge and reattaches on the leeward face, giving rise to a clockwise rotating recirculation vortex. This vortex grows along the leeward face, fed by circulation generated at the separation point on the upper face and entrained into the base region. The vortex grows until it covers the entire leeward face, at which point the separation streamline interferes with the opposing shear layer from the lower face. As a result, a saddle point forms along the lower shear layer downstream of the obstacle and cuts off the flow of circulation from the lower separation point to the counter-clockwise rotating vortex in the base region. This vortex subsequently sheds.

The bottom shear layer now reattaches along the lower face of the cylinder and a counter-clockwise recirculation vortex begins to grow upward along the leeward face. This new vortex displaces the clockwise vortex into the base region. The clockwise vortex is still fed by circulation from the upper shear layer and thus continues to grow as well. However, the counter-clockwise vortex eventually extends over the entire leeward face and interferes with upper shear layer, thereby cutting off the flow of circulation to the clockwise vortex,

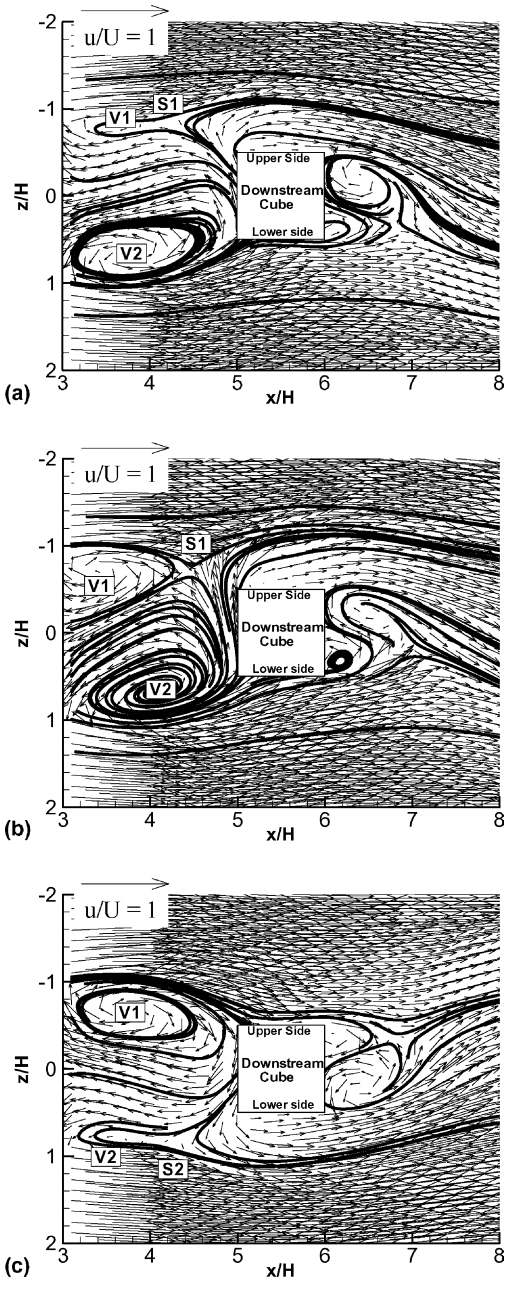

Fig. 5. Phase-averaged vector representation of the $\langle u \rangle - \langle w \rangle$ velocity components in the plane $y/H = 0.25$ for phases (a) $\phi = 0°$, (b) $\phi = 54°$ and (c) $\phi = 162°$.

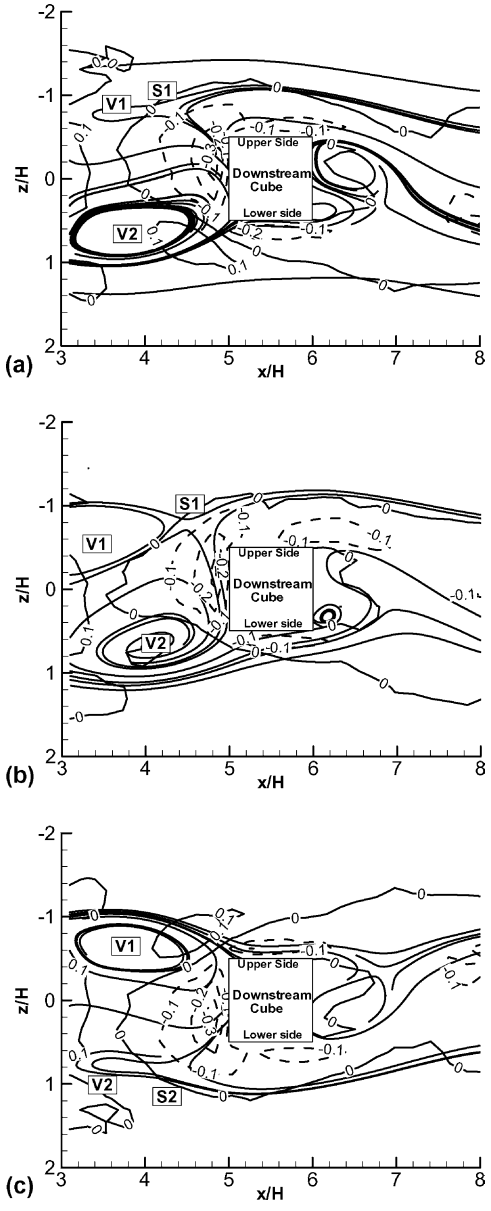

Fig. 6. Phase-averaged contour representation of the vertical, $\langle v \rangle$, velocity component in the plane $y/H = 0.25$ for phases (a) $\phi = 0°$, (b) $\phi = 54°$ and (c) $\phi = 162°$. $\langle v \rangle$ is normalized by U: (- - -) negative values, (—) positive values; contour interval 0.01.

which then sheds. The upper shear layer reattaches on the upper face and the cycle is repeated.

The shedding process for the tandem, surface-mounted cube geometry is shown in Figs. 5 and 6 for selected phases of the shedding cycle. The phase averaged streamwise, $\langle u \rangle$, and spanwise, $\langle w \rangle$, velocity components in the plane $y/H = 0.25$ are shown as vectors in Fig. 5, while the contours representing the vertical velocity component, $\langle v \rangle$, in Fig. 6. The flow field topology is found to be similar for all horizontal planes $0.05 < y/H < 0.75$. However, it is observed that the location of the nodes and saddles for a given phase differ slightly between planes, indicating that the rotation axis of the flow structures is slightly tilted relative to a vertical axis. Note that the results are presented in an absolute frame of reference and the sectional streamtraces are included as visual aids.

Significant differences between the two- and three-dimensional shedding processes are seen by inspection of Fig. 5. Unlike the two-dimensional case, well-developed recirculation vortices are observed in the base region of the upstream obstacle for all phases. Phase 1 ($\phi = 0°$, Fig. 5a) is arbitrarily defined as the phase of the shedding cycle immediately after the upper vortex has shed. A saddle point, $S1$, is located directly downstream of the upper base vortex, $V1$. Note that there is a strong vertical down flow along the front face of the downstream cube (Fig. 6(a)). The dividing streamtrace along the lower shear layer impinges on the cube corner. The flow is attached along the lower side of the cube. Circulation is fed to the counter-clockwise base vortex $V2$ and both $V1$ and $V2$ continues to grow as shown in Fig. 5(b), $\phi = 54°$. In this phase, the spanwise flow along the front face is directed towards the upper edge ($\langle w \rangle < 0$) and the core of the region of strong (downward, $\langle v \rangle < 0$) vertical flow, shown in Fig. 6(b), reaches its maximum z-excursion and maximum $\langle v \rangle$ velocities are located near the upper cube corner.

The core of the vortex $V2$ and the saddle point $S1$ move downstream until the location of $S1$ coincides with the upper leading edge corner of the downstream cube. There is a rapid switch in the direction of the spanwise flow, within a shedding phase difference of $\Delta\phi = 20°$, towards the lower leading edge and the vertical stream moves towards the lower leading edge, as in Fig. 6(c) for $\phi = 162°$, to interfere with the bottom shear layer flow causing the appearance of a saddle point, and a counter-clockwise vortex sheds. At this phase of the shedding cycle, the dividing streamline along the upper shear layer now impinges on the leading corner of the downstream cube, while the lower shear layer no longer attaches on the obstacle lower face. In Fig. 5(c), $\phi = 162°$, the saddle point $S2$ is clearly visible, the vortex $V2$ is reduced in size and the top vortex, $V1$, penetrates deeply into the inter-obstacle cavity. The half-cycle is then repeated, but 180° out of phase, to lead to the shedding of $V1$.

Contrary to the two-dimensional case, the vortices $V1$ and $V2$ are not completely shed. Rather, only part of the circulation is convected downstream in the shed vortices. Immediately after the upper shedding event, the remnant core for $V1$ is still visible in the upper half of the flow plane (Fig. 5(a), $\phi = 0°$). Similarly, the remnant core for $V2$ is also observed for $\phi = 162°$ (Fig. 5(c)).

The mechanism triggering shedding is different for the two- and three-dimensional geometries. In the classical (two-dimensional) model, the vortex growing along the cylinder face in the base region and eventually extends across the leeward face to interfere with the opposing

shear layer, thereby cutting off the flow of circulation to the opposite-rotating vortex in the base region, causing it to shed completely. For the present three-dimensional case, however, it is the stream of strong vertical flow along the face of the second cube, which moves towards the bottom leading edge. The vertical stream thus appears to split the vortex, which is partly shed, while the remainder begins to grow again.

4. Discussion

Some important differences between the random (turbulent) contributions to the fluctuations are observed between results for the shedding of the three-dimensional, tandem geometry and the classical two-dimensional (square) cylinder of Lyn et al. (1995). The turbulent kinetic energy, $\langle k \rangle$, and the Reynolds shear stress, $\langle u'w' \rangle$, in the plane $y/H = 0.25$ are shown in Figs. 7 and 8, respectively, for the phases $\phi = 0°$ and $\phi = 54°$. Immediately after the shedding of the upper vortex ($\phi = 0°$, Fig. 7(a)), large values of $\langle k \rangle$ are concentrated along the windward face of the downstream cube and along the shear layer, extending from the vortex $V2$

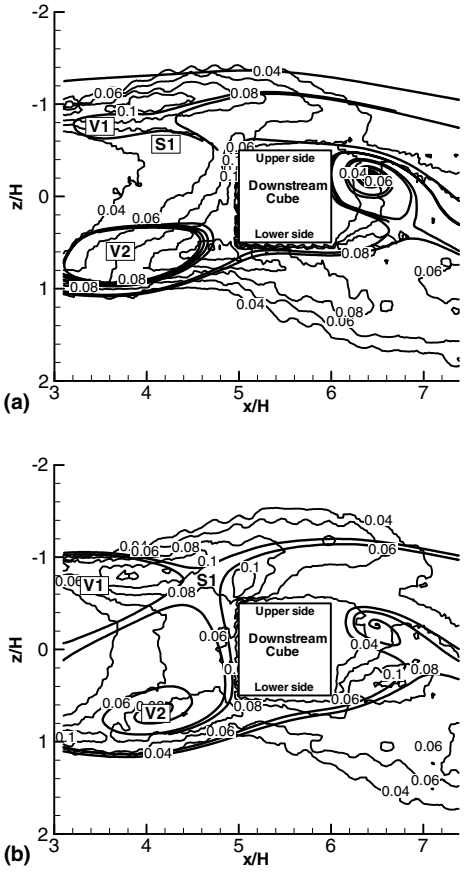

Fig. 7. Contours of the random contribution to the turbulent kinetic energy, $\langle k \rangle$, for phases (a) $\phi = 0°$ and (b) $\phi = 54°$. $\langle k \rangle$ is normalized by U^2: contour interval 0.02.

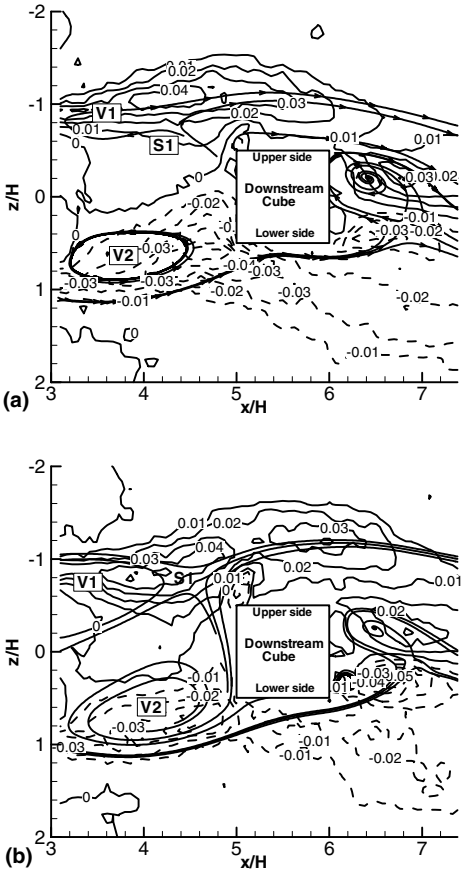

Fig. 8. Contours of the random contribution to the turbulent shear stress $\langle u'w' \rangle$ for the phases (a) $\phi = 0°$ and (b) $\phi = 54°$. $\langle u'w' \rangle$ is normalized by U^2: (- - -) negative values, (—) positive values; contour interval 0.01.

downstream past the cube. The $\langle k \rangle$ values are large along the upper shear layer in the vicinity of the remnant core, $V1$, while about the saddle point $S1$, $\langle k \rangle$ is significantly smaller. The $\langle u'w' \rangle$-distribution for $\phi = 0°$ is shown in Fig. 8(a). Again, large values occur along the shear layers. However, unlike for $\langle k \rangle$, large (absolute) values are also observed in the vicinity of the saddle points.

For the single obstacle, two-dimensional geometry at an equivalent phase in the shedding cycle, the turbulent field distribution in the formation region shows some similarity: the maximum magnitude for $\langle k \rangle$ and $\langle u'w' \rangle$ is similar and concentrated along the shear layers. Close to the plane of symmetry, $z/H = 0$, and downstream of the saddle point, $S1$, $\langle w \rangle$ is small while $\langle k \rangle$ is large.

For phase $\phi = 54°$ (Figs. 7(b), 8(b)), the lower vortex penetrates deeply in the cavity. High $\langle k \rangle$ values are concentrated about the vortex cores and close to the upper leading corner of the downstream cube, where the vertical stream interferes with the upper shear layer. Along the front face of the obstacle, $\langle k \rangle$ is generally lower, while $\langle u'w' \rangle$ is much larger than for $\phi = 0°$. In this phase, $\langle w \rangle$ is large. For the equivalent phase for the

two-dimensional geometry, Lyn et al. (1995) observe that about $z/H = 0$, both $\langle k \rangle$ and $\langle u'w' \rangle$ are low in magnitude. They argue that the large $\langle w \rangle$ component convects "free stream" fluid into the base region, resulting in lower turbulence levels. For the three-dimensional geometry, $\langle k \rangle$ does not decrease as significantly and $\langle u'w' \rangle$ increases in magnitude, being close to an absolute maximum as $\langle w \rangle$ reaches its maximum.

Lyn et al. (1995) analysed the $\langle k \rangle$-production term:

$$\langle P \rangle = -\langle u'^2 \rangle \frac{\partial \langle u \rangle}{\partial x} - \langle w'^2 \rangle \frac{\partial \langle w \rangle}{\partial z} - \langle u'w' \rangle \left(\frac{\partial \langle u \rangle}{\partial z} + \frac{\partial \langle w \rangle}{\partial x} \right),$$

for the two-dimensional square cylinder geometry in the base region. An excerpt of their results is shown in Fig. 9, where $\langle P \rangle$-contours are shown for a phase corresponding approximately to phase $\phi = 0°$ in this study. Note that the symbols + and × denote the location of vortex cores and vorticity saddles, respectively. The $\langle P \rangle$-contours form a neck from one side of the cylinder to the other between forming vortices. These features are related to large differences in $\langle u'^2 \rangle$ and $\langle w'^2 \rangle$ and large $\partial \langle u \rangle / \partial x$. These regions of high $\langle P \rangle$ are associated with bursts of large $\langle k \rangle$ observed between shed vortices. Peak production terms are also observed near, but distinctly away, from the location of saddle points. These peaks result mainly from shear contribution to the production term and coincide with peaks in $\langle u'w' \rangle$.

For the present geometry, $\langle P \rangle$-contours are shown in Fig. 10 for $\phi = 0°$ and 54°. Similarly to the two-dimensional case, concentrations of large $\langle P \rangle$ values are observed along the shear layers. However, in the cavity (i.e. formation or base) region, major differences to the two-dimensional case are observed. For example, the contours do not form a neck across the base region and production levels in the cavity region remain generally low throughout the shedding cycle. This difference is probably due to the presence of the downstream cube, which limits the magnitude of $\partial \langle u \rangle / \partial x$. Thus the large values of $\langle k \rangle$ observed in the cavity region are principally generated in the shear layers and convected into

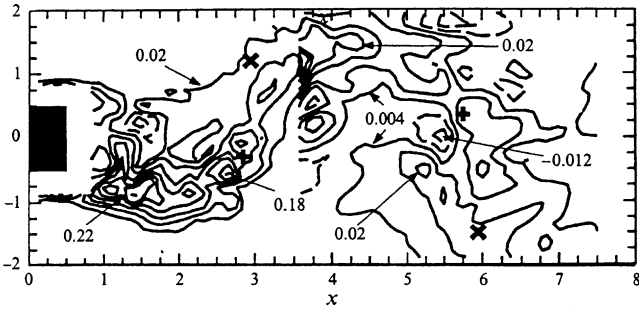

Fig. 9. Contour plots of $\langle P \rangle$ at phase (9, 19) downstream of a square cylinder as adapted from Lyn et al. (1995). The shedding phase corresponds approximately to phase $\phi = 0°$ in this study. Symbols + and × denote vortex cores and vorticity saddle points, respectively. Contour intervals for $x < 3.5$ are 0.04 and for $x > 3.5$, 0.008.

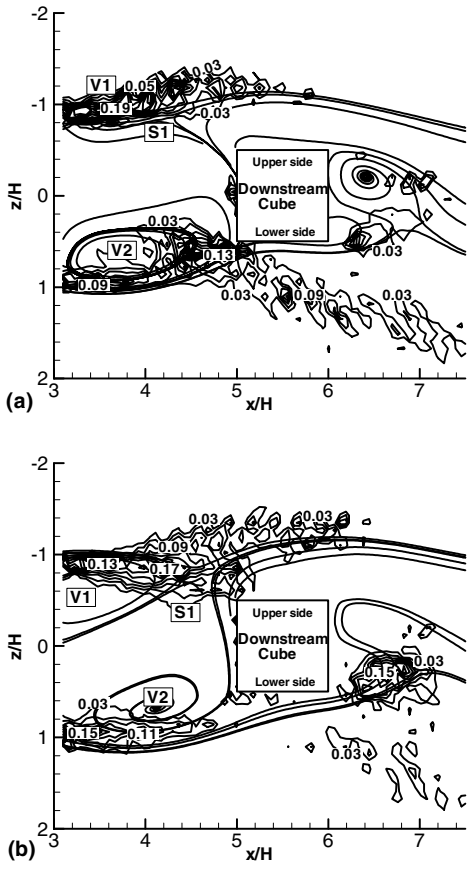

Fig. 10. Contours of the normalized $\langle k \rangle$-production terms, $\langle P \rangle$, in the plane $y/H = 0.25$: (a) $\phi = 0°$, (b) $\phi = 54°$. $\langle P \rangle$ is normalized by U^3/H; contour interval 0.02.

and across the cavity. In Fig. 7(b) for $\phi = 54°$, the concentration of large $\langle k \rangle$ seen at the upper corner is convected downstream at the same time as the lower vortex is shed, thus creating a high $\langle k \rangle$-burst in-phase with the passage of the vortex. In contrast, for the two-dimensional case, the $\langle k \rangle$-burst is generated locally between the vortices.

Unlike the two-dimensional case, peak production rates do not coincide with peak $\langle u'w' \rangle$ in the cavity. These differences are expected to result from three-dimensional effects, since the major differences are observed upstream of the second cube, where vertical gradients and $\langle v \rangle$ are largest.

5. Concluding remarks

In the two-dimensional case, shedding is triggered by the interference between the forming vortex and the opposite shear layer. For three-dimensional geometries in the locked regime, the vortex sheds as a result of the interference between the vertical stream along the front face of the downstream obstacle and the side shear layers. The opposite vortex induces the spanwise flow

across the face of the downstream cube, which provides the opposing shear layer coupling necessary for stable, periodic shedding. It thus appears reasonable to expect that the shedding frequency will scale linearly with the obstacle spacing, since the shedding of the vortex is triggered by the vertical stream and that the location of this stream is determined by the location of the second obstacle. When the obstacle spacing is increased sufficiently, the top shear layer attaches upstream of the downstream obstacle, eliminating the vertical stream and a locked regime is no longer possible. The vertical stream is a three-dimensional effect and does not exist for two-dimensional tandem arrangements, which may explain why a locked regime has not been observed in these cases.

References

Albrecht, T., Barnes, F.H., Baxendale, A.J., Grant, I., 1988. Vortex shedding from two cylinders in tandem. J. Wind Eng. Ind. Aero. 28, 201–208.

Benedict, L.J., Gould, R.D., 1996. Towards better uncertainty for turbulent statistics. Exp. Fluids 107, 161–164.

Castro, I.P., Robins, A.G., 1977. The flow around a surface-mounted cube in uniform and turbulent streams. J. Fluid Mech. 79Z, 307–335.

Edwards, R.V., 1987. Report of the special panel on statistical particle bias problems in laser anemometry. Trans. ASME, J. Fluids Eng. 109, 89–93.

Gaydon, M., Rockwell, D., 1999. Vortices incident upon oscillating cylinder: Flow structure and loading. J. Fluids Struct. 13, 709–722.

Hangan, H., Vickery, B.J., 1999. Buffeting of 2D (sharp-edged) bluff bodies. J. Wind Eng. Ind. Aero. 82, 173–187.

Havel, B., Hangan, H., Martinuzzi, R., 2001. Buffeting for 2D and 3D sharp-edged bluff bodies. J. Wind Eng. Ind. Aero. 89, 1369–1381.

Lyn, D.A., Einav, S., Rodi, W., Park, J.H., 1995. A laser-Doppler velocimetry study of ensemble-averaged characteristics of the turbulent near wake of a square cylinder. J. Fluid Mech. 304, 285–319.

Martinuzzi, R., Havel, B., 2000. Turbulent flow around two interfering surface-mounted cubic obstacles in tandem arrangement. Trans. ASME, J. Fluids Eng. 122, 24–31.

Okajima, A., 1982. Strouhal numbers of rectangular cylinders. J. Fluid Mech. 123, 379–398.

Ricciardelli, F., 1994. Aerodynamics of a pair of square cylinders, M.E.Sc. Thesis. The University of Western Ontario, London, Ontario, Canada.

Rockwell, D., 1998. Vortex body interactions. Ann. Rev. Fluid Mech. 30, 199–229.

Rudoff, R.C., Bachalo, W.D., 1991. Seed Particle Response and Size Characterization in High Speed Flows. Proc. ASME Fluids Eng. Conf., Symp. on Laser Anem., Adv., Appl. 2, 443–447.

Sakamoto, H., Haniu, H., 1988. Aerodynamic forces acting on two square prisms placed vertically in a turbulent boundary layer. J. Wind Eng. Ind. Aero. 31, 41–66.

Williamson, C.H.K., 1996. Vortex dynamics in the cylinder wake. Ann. Rev. Fluid Mech. 28, 477–539, Ann. Rev. in Fluid Mech. 30, 199–229.

Zdravkovich, M.M., 1977. Review of flow interference between two circular cylinders in various arrangements. Trans. ASME, J. Fluids Eng. 99, 618–633.